PCCP

Accepted Manuscript




ROYAL SOCIETY OF CHEMISTRY

www.rsc.org/pccp

Chemical Science

RSCPublishing

COMMUNICATION

# Durability, inactivation and regeneration insight of silver tetratantalate in photocatalytic $H_2$ evolution

Cite this: DOI: 10.1039/x0xx00000x

Hongjun Dong,[ab] Gang Chen,*[a] Jingxue Sun,*[a] Chunmei Li,[a] Chade Lv[a] and Yidong Hu[a]

Received 00th January 2014,
Accepted 00th January 2014

DOI: 10.1039/x0xx00000x

www.rsc.org/

**The prepared $Ag_2Ta_4O_{11}$ photocatalyst exhibits the durable $H_2$-production activity from the water. We deeply have an insight into the durability, inactivation and regeneration mechanism. This work provides a new perspective and makes an important step for the research of Ag-based photocatalysts.**

Photocatalytic $H_2$ evolution from the water has been regarded as one of the promising techniques due to the water available and renewable solar resource.[1] In recent years, most Ag-based compounds were widely reported and served as a kind of effective photocatalysts because unique electronic configurations of $Ag^+$ ions can participate in composition and hybridization of energy band structure.[2] They usually are applied to decomposing organic pollutants and $O_2$ evolution from the water under light irradiation. In contrast, there have been only a few reports on applying them to $H_2$ evolution from the water. We know that most Ag-based photocatalysts are very sensitive to light thus they unavoidably suffer from photocorrosion, leading to decreased photocatalytic activity and shortened operation life. Up to now, the requisite durability and regeneration ability of photocatalysts are rarely considered, which are significant to recycling use. Recently, $Rh_{2-y}Cr_yO_3$/GaN:ZnO reported by Domen et al. presents the excellent long-term stable $H_2$ evolution activity and regeneration ability,[3] which provides feasibility and bright prospect for the application of photocatalysts to $H_2$-production. However, as far as Ag-based photocatalysts are concerned, realizing their durable operation and regeneration is still a tremendous challenge.

In this work, the prepared $Ag_2Ta_4O_{11}$ photocatalyst shows the durable $H_2$-production activity from the water lasting for several days under the simulated sunlight provided by an unfiltered Xe lamp. Importantly, the used sample can realize regeneration by a simple re-calcination process and its corresponding $H_2$ evolution activity almost recovers the level of fresh sample. We deeply have an insight into the durability, inactivation and regeneration mechanism.

From the amount of photocatalytic $H_2$-production over the fresh $Ag_2Ta_4O_{11}$ sample in Fig. 1a, the average rate reaches to ~23.1 μmol $h^{-1}$ $g^{-1}$ within 5 h. It indicates that $Ag_2Ta_4O_{11}$ can serve as a photocatalyst in $H_2$-production from the water. Moreover, cycle operations of the sample (Fig. 1b) displays that the $H_2$-production yield has no obvious reduction in the fifth day and reaches to ~80% of the level of fresh sample. In addition, the stability in the air using an 'interval experiment' method is shown in Fig. 1c. After enduring the irradiation of 30 days, the irradiated sample still maintains a stable $H_2$ evolution rate although its $H_2$-production yield is only ~30% of the level in the first day. More importantly, after the used sample undergoes a simple re-calcination process, $H_2$ evolution activity of the regenerated sample almost achieves the level of fresh sample (Fig. 1a). All above results indicate that $H_2$ evolution of the $Ag_2Ta_4O_{11}$ sample exhibits eminently durable operation and activity recovery ability, which is very hard-won compared with most Ag-based photocatalysts. Meanwhile, the specific surface areas of the fresh, used and regenerated samples are tested, which are 0.9426 $m^2$ $g^{-1}$, 1.3614 $m^2$ $g^{-1}$ and 1.2148 $m^2$ $g^{-1}$, respectively. The approximate values of the specific surface area indicate that it has not direct influence on the photocatalytic activity.

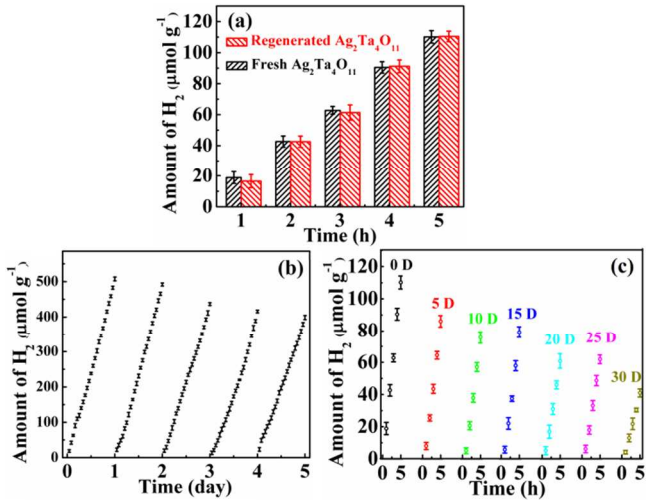


**Fig. 1** $H_2$-production amount of the fresh and regenerated samples (a), circle operations of $H_2$ evolution (b, c).

In order to understand deeply the durability, inactivation and regeneration mechanism of $Ag_2Ta_4O_{11}$ sample in $H_2$ evolution, the XRD (X-Ray Diffraction), SEM (Scanning Electron Microscope), TEM (Transmission Electron Microscopy) and XPS (X-ray Photoelectron Spectroscopy) et al. analyses are further performed. The XRD of the fresh sample (Fig. 2a) coincides with standard and simulated patterns and the diffraction peaks are strongly sharp, which reveals that the sample is pure and well-crystallized. After 1 and 5 days of photocatalytic reaction, the white sample turns to grey but the XRD patterns (Fig. 2b-c) are almost unchanged, which suggests that the photocorrosion is a slow process. When the sample suspended in water endures irradiation of 30 days in the air (Fig. 2d) and then is performed $H_2$ evolution of 5 h (Fig. 2e), there still are no other phases appearing in the XRD patterns. It further demonstrates that $Ag_2Ta_4O_{11}$ is a relatively durable Ag-based photocatalyst. Furthermore, after the used sample undergoes a re-calcination process, the only pure $Ag_2Ta_4O_{11}$ phase is detected (Fig. 2f) and the grey sample changes into white again, which implies that the sample may restore to its original state, thus realizing regeneration. These are supported by the results of TEM and XPS analyses, as will be shown below.

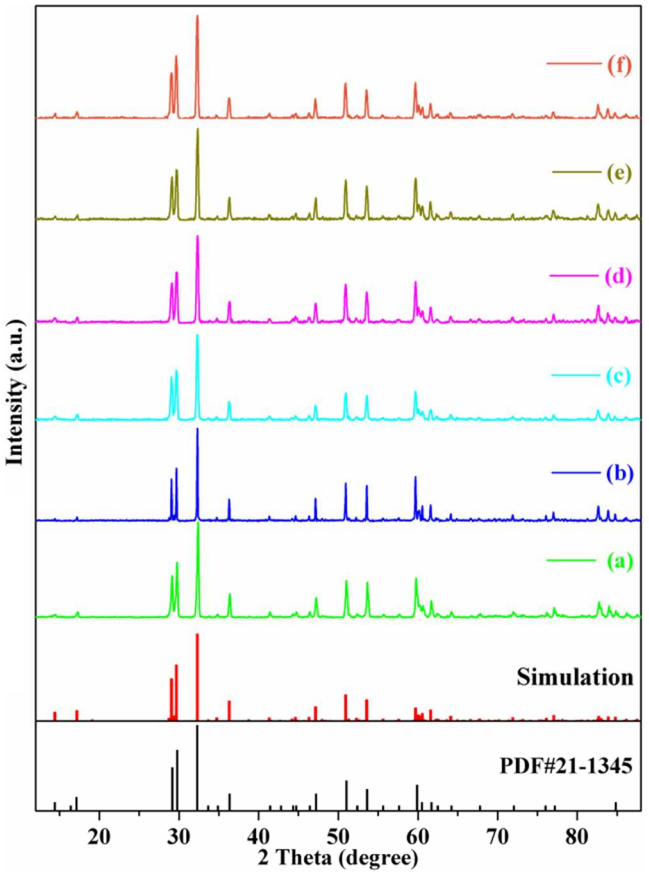


**Fig. 2** XRD patterns of the $Ag_2Ta_4O_{11}$ sample, fresh sample (a), sample reacting 1 day (b) and 5 days (c), sample suspended in water enduring irradiation of 30 days under the simulated sunlight in the air (d), sample operating $H_2$ evolution of 5 h after irradiation of 30 days (e) and sample undergoing re-calcination for the used photocatalyst (f).

The SEM (Fig. 3a) and TEM (Fig. 3b) images show that the fresh $Ag_2Ta_4O_{11}$ sample exhibits irregular bulk distribution. The HRTEM (High Resolution Transmission Electron Microscopy) image (Fig. 3c) of the fresh sample displays that the interplanar spacing d=0.614 nm agrees well with (006) crystal plane in hexagonal $Ag_2Ta_4O_{11}$ crystal. The FFT (Fast Fourier Transform) pattern in Fig. 3d shows some distinctly symmetrical diffraction spots, which indicates that the fresh sample exhibits single crystal characteristic. After $H_2$ evolution is performed, the abundant nanoparticles with diameter of 5-20 nm are generated on the used sample surface according to the TEM image (Fig. 3e). The SAED (Selected Area Electron Diffraction) pattern (Fig. 3f) performed on the bulk shows two groups of diffraction spots, in which the marked spots belong to (006) and (113) crystal planes of $Ag_2Ta_4O_{11}$ as well as (111) and (200) crystal planes of metal Ag, respectively. It indicates that the photocorrosion is Ag generation process on the sample surface resulting from the reducing action of photogenerated electrons. This result is further evidenced by HRTEM image (Fig. 3g). The interplanar spacing d values of bulk and nanoparticle are 0.614 nm and 0.233 nm, which is in line with (006) crystal planes of $Ag_2Ta_4O_{11}$ and (111) crystal planes of meal Ag, respectively. Moreover, after the used sample undergoes a re-calcination process, TEM image (Fig. 3h) and SAED pattern (the insert of Fig. 3h) show that the surface Ag nanoparticles vanish and the single symmetric diffraction spots appear, respectively. Meanwhile, the interplanar spacing d value of 0.307 nm in HRTEM image (Fig. 3i) corresponds to (00 12) crystal planes of $Ag_2Ta_4O_{11}$. It indicates that the pure $Ag_2Ta_4O_{11}$ sample is obtained again, which evidences that the used sample realizes regeneration.

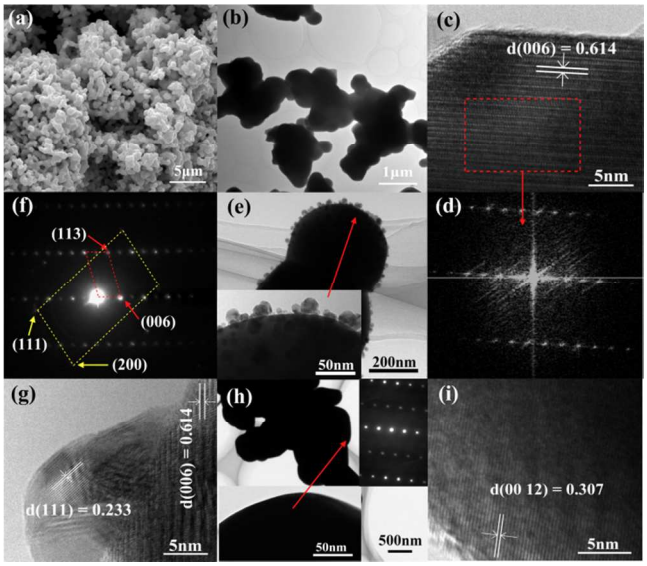


**Fig. 3** SEM (a), TEM (b), HRTEM (c) images, FFT pattern (d) of the fresh sample; TEM image (e), SAED pattern (f) HRTEM image (g) of the used sample; TEM image (h), SAED pattern (the insert of h) and HRTEM (i) image of the regenerated sample.

The surface elements and valence state variation of the $Ag_2Ta_4O_{11}$ sample before and after reaction are investigated by XPS. From XPS spectra (Fig. 4a) of the fresh sample, two overlapped O 1s peaks at 530.1 eV and 531.7 eV suggest that oxygen has two different chemical states,[4] which belong to lattice $O^{2-}$ in the sample surface and adsorbed hydroxyl species, respectively.[5] The binding energy peaks at 25.7 eV and 27.7 eV attribute to $4f_{7/2}$ and $4f_{5/2}$ states of lattice $Ta^{5+}$ in the sample surface. Notably, the peaks assigned respectively to $3d_{5/2}$ and $3d_{3/2}$ states of silver at 367.8 eV and 373.6 eV exhibit symmetric shapes, which indicates that silver may only possess one $Ag^+$ chemical state.[4] After $H_2$ evolution is performed, no shifting peaks of $Ta^{5+}$ in Fig. 4b indicate that the chemical state of tantalum is unchanged and unrelated to the photocorrosion. In contrast, besides binding energy peaks of lattice $Ag^+$ in $Ag_2Ta_4O_{11}$, the shoulder peaks are observed at 368.5 eV and 374.5 eV in the

XPS spectrum of Ag (Fig. 4b), which derive from metal Ag $3d_{5/2}$ and $3d_{3/2}$ states, respectively. It further evidences that metal Ag generates on the sample surface in $H_2$ evolution process. In addition, the lattice $O^{2-}$ 1s peak at 529.8 eV shifts 0.3 eV towards low binding energy compared with that of the fresh sample (530.1 eV), which may be caused by a slight chemical state change of lattice O owing to mental Ag generation on the sample surface at the $H_2$ evolution process. Meanwhile, the peak at 531.7 eV is obviously enhanced, which implies the oxygen content of hydroxyl species increasing. It is the reasonable result that, hydroxyl ($OH^-$) are produced on the sample surface after releasing $H_2$ from the $H_2O$ molecules, which can be oxidized by holes to hydroxyl radical (·OH) owing to the more positive valence band position (3.82 eV, Table S1†) than that of ·OH/$HO^-$ couple (2.38 eV vs NHE),[6] finally resulting in peroxidation effect. Furthermore, when the used sample undergoes a simple re-calcination, the XPS spectra (Fig. 4c) almost recover original state. The peak positions of $Ta^{5+}$, $Ag^+$ and $O^{2-}$ all are in accord with that of the fresh sample and the shoulder peaks coming from metal Ag vanish, which evidences that the used sample achieves regeneration.

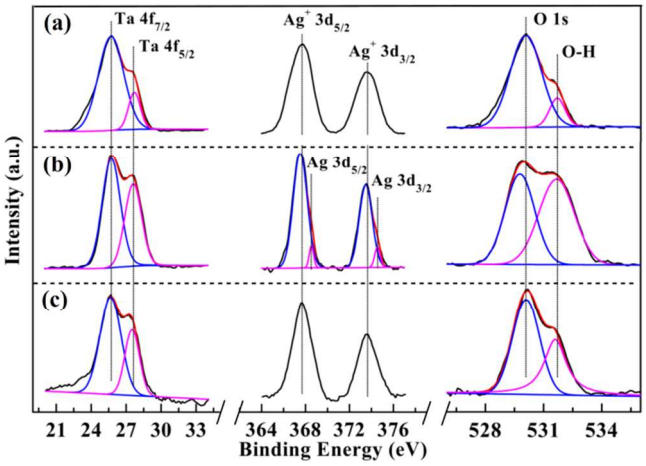


**Fig. 4** XPS spectra of the fresh sample (a), used sample (b) and regenerated sample (c).

The activity and stability of photocatalyst are determined by its electronic and crystal structure in essence. The theoretical calculation for $Ag_2Ta_4O_{11}$ is performed based on *ab* initio density functional theory (ESI†). The energy band diagram of $Ag_2Ta_4O_{11}$ (Fig. 5a) confirms its indirect transition characteristic. The relative flat conduction band bottom and valence band top imply that $Ag_2Ta_4O_{11}$ can produce a direct transition by only a little high energy,[7] which signifies that electrons on the valence band are easily excited to the conduction band, thus improving photocatalytic activity. The density of states (DOS) shows that the valence band of $Ag_2Ta_4O_{11}$ is mainly composed of the hybridized Ag 4d and O 2p orbits. The high degree of overlap state indicates that the intense bonding effect exists between Ag 4d and O 2p orbits, which contributes to improving the stability of $Ag_2Ta_4O_{11}$. The conduction band of $Ag_2Ta_4O_{11}$ is mainly composed of Ta 5d orbit with a little O 2p and Ag 5s states. The mobility of charge carriers is inverse ratio to their effective mass, thus a little Ag 5s state in the conduction band can reduce electronic effective mass and increase delocalization to improve photocatalytic ability.[2b, 8]

The crystal structure of $Ag_2Ta_4O_{11}$ is similar to that of reported $Ag_2Nb_4O_{11}$.[4] As shown in Fig. 5b, the alternate $TaO_6$ and $AgO_6$ octahedrons as well as $TaO_7$ pentagonal bipyramids constitute a polyhedron layer in X-Y plane, respectively. Two polyhedron layers alternately stack along Z-axis by corner-connecting to construct the 3D framework. For the plenty of layered photocatalysts, this alternate layered structure avails the separation and transport of charge carriers.[9] In $Ag_2Ta_4O_{11}$ crystal, the photogenerated electrons and holes easily migrate and separate between the hybridized Ag 4d and O 2p orbits as well as the unoccupied Ta 5d orbits in the interlaced network layer of $AgO_6$ and $TaO_6$ octahedrons in X-Y plane. The bond angle of Ta-O-Ta is 180° in $TaO_6$ octahedron, which benefits migration of charge carriers in its framework.[10] In addition, the bond angle of O-Ta-O also reaches to 135.5° between $TaO_6$ and $TaO_7$ units, which conduces to electron transfer in two layers. The unique $TaO_7$ pentagonal bipyramid layers can form a transportation channel of electrons to enhance the transfer and separation ability of electron-hole pairs. Importantly, the $AgO_6$ octahedron plays a crucial role for the stability of $Ag_2Ta_4O_{11}$, in which the central Ag atom is linked to adjacent six O atoms. It restrains efficiently that $Ag^+$ ions dissociate from $Ag_2Ta_4O_{11}$ crystal by forming intense coordinate bond between Ag and O atom, thus avoiding reduction of $Ag^+$ ions by photogenerated electrons to maximum extent. Additionally, the same layer $TaO_6$ units and near layer $TaO_7$ units may rapidly transfer the electrons generated in $AgO_6$, which can also separate electrons and inhibit the reduction of lattice $Ag^+$ ions in the crystal structure.

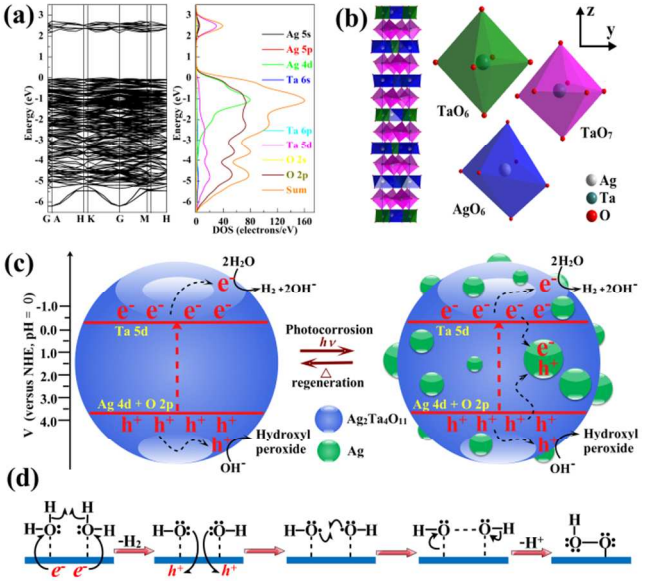


**Fig. 5** Energy band diagram and DOS of $Ag_2Ta_4O_{11}$ (a), crystal structure of $Ag_2Ta_4O_{11}$ (b) and the possible reaction mechanism and carriers transfer behavior (c and d).

Based on above analyses, the possible reaction mechanism and carriers transfer behaviour are illustrated in Fig. 5c, d. When the sample is exposed to the simulated sunlight, electron-hole pairs are firstly produced in $AgO_6$ octahedrons. The electrons and holes transfer to conduction band composed of dominant Ta 5d orbit and valence band composed of hybridized Ag 4d and O 2p orbits, respectively. In consequence, the electron transport channel is formed in interlaced network constructed by $TaO_6$ and $TaO_7$ as well as the hole transport channel is formed in $AgO_6$, respectively. The electrons and holes migrate to the sample surface *via* their transport channel and then participate in photocatalytic reaction, respectively. In fact, the $H_2$ generation reaction is an oxidation-reduction process of $H_2O$ molecules absorbed on the sample surface. As shown in Fig. 5d, the photogenerated electrons immediately react with the $H_2O$ to

release $H_2$ and produce hydroxyl ($OH^-$) on the sample surface. Then hydroxyl can be further oxidized by holes to hydroxyl radical (·OH). Lastly the adjacent two hydroxyl radicals immediately react with each other to generate $H_2O_2$, which release a $H^+$ ion to form hydroxyl peroxide on the sample surface, resulting in surface oxygen content increase. The peroxidation phenomenon also appears on other tantalates.[11] Furthermore, when the used sample further undergoes a re-calcination process, the hydroxyl peroxide on the sample surface may decompose to be hydroxyl afresh and revert to the original state, which achieves the dual recovery of photocatalyst and activity. We should point out that the abundant Ag nanoparticles are generated owing to reducing action of the photogenerated electrons, which can cover on the sample surface to reduce the light harvest ability because of their shielding effect and serving as charge carrier recombination centres, leading to activity reduction of photocatalyst.

## Conclusions

In conclusion, the Ag-based photocatalyst $Ag_2Ta_4O_{11}$ exhibits the durable $H_2$ evolution activity up to 5 days under the simulated sunlight. Even though the sample in water undergoes the continuous irradiation of 30 days under the simulated sunlight, the irradiated sample still maintains a stable $H_2$ evolution rate. More importantly, the used sample can realize regeneration by a re-calcination process and its $H_2$ evolution activity almost recovers the level of fresh sample. We have deeply insight into the durability, inactivation and regeneration mechanism using various measure techniques and combining with electronic and crystal structure analyses. This work provides a new perspective and makes an important step for the research of Ag-based photocatalysts.

## Acknowledgment

This work was financially supported by the National Nature Science Foundation of China (21071036, 21271055 and 21471040) and Province Natural Science Foundation of Heilongjiang Province (ZD201011). We acknowledge for the support by Open Project of State Key Laboratory of Urban Water Resource and Environment，Harbin Institute of Technology (No. QAK201304) and Program for Innovation Research of Science in Harbin Institute of Technology.

## Notes and references

[a] Department of Chemistry, Harbin Institute of Technology, Harbin 150001, P. R. China.

[b] Department of Chemistry, Baicheng Normal University, Baicheng 137000, P. R. China.

†Electronic Supplementary Information (ESI) available: [Detailed description of the synthesis, characterization methods, theoretical calculation and light absorption property of the sample]. See DOI: 10.1039/c000000x/

1 (a) F. E. Osterloh, *Chem. Soc. Rev.*, 2013, **42**, 2294-2320; (b) X. Wang, Q. Xu, M. Li, S. Shen, X. Wang, Y. Wang, Z. Feng, J. Shi, H. Han and C. Li, *Angew. Chem. Int. Ed.*, 2012, **51**, 13089-13092; (c) P. Zhang, J. Zhang and J. Gong, *Chem. Soc. Rev.*, 2014, **43**, 4395-4422; (d) Q. Jia, A. Iwase and A. Kudo, *Chem. Sci.*, 2014, **5**, 1513-1519.

2 (a) X. K. Li, S. X. Ouyang, N. Kikugawa and J. H. Ye, *Appl. Catal. A: Gen.*, 2008, **334**, 51-58; (b) S. X. Ouyang and J. H. Ye, *J. Am. Chem. Soc.*, 2011, **133**, 7757-7763; (c) Z. G. Yi, J. H. Ye, N. Kikugawa, T. Kako, S. X. Ouyang, H. Stuart-Williams, H. Yang, J. Y. Cao, W. J. Luo, Z. S. Li, Y. Liu and R. L. Withers, *Nat. Mater.*, 2010, **9**, 559-563; (d) H. J. Dong, G. Chen, J. X. Sun, C. M. Li, Y. G. Yu and D. H. Chen, *Appl. Catal. B: Environ.*, 2013, **134-135**, 46-54; (e) W. Yang, L. Zhang, Y. Hu, Y. Zhong, H. B. Wu and X. W. (David) Lou, *Angew. Chem. Int. Ed.*, 2012, **51,** 11501-11504; (f) Y. X. Tang, Z. L. Jiang, G. C. Xing, A. R. Li, P. D. Kanhere, Y. Y. Zhang, T. C. Sum, S. Z. Li, X. D. Chen, Z. L. Dong and Z. Chen, *Adv. Funct. Mater.*, 2013, **23**, 2932-2940; (g) Y. S. Xu and W. D. Zhang, *ChemCatChem*, 2013, **5**, 2343-2351; (h) J. T. Tang, Y. H. Liu, H. Z. Li, Z. Tan and D. T. Li, *Chem. Commun.*, 2013, **49**, 5498-5500; (i) C. Hu, T. W. Peng, X. X. Hu, Y. L. Nie, X. F. Zhou, J. H. Qu and H. He, *J. Am. Chem. Soc.*, 2010, **132**, 857-862.

3 T. Ohno, L. Bai, T. Hisatomi, K. Maeda and K. Domen, *J. Am. Chem. Soc.*, 2012, **134**, 8254-8259.

4 H. Dong, G. Chen, J. Sun, Y. Feng, C. Li and C. Lv, *Chem. Commun.*, 2014, **50**, 6596-6599.

5 J. B. Mu, C. L. Shao, Z. C. Guo, Z. Y. Zhang, M. Y. Zhang, P. Zhang, B. Chen and Y. C. Liu, *ACS Appl. Mater. Interfaces*, 2011, **3**, 590-596.

6 H. Cheng, B. Huang, Y. Dai, X. Qin and X. Zhang, *Langmuir*, 2010, **26**, 6618-6624.

7 U. A. Joshi and P. A. Maggard, *J. Phys. Chem. Lett.*, 2012, **3**, 1577-1581.

8. Y. Hosogi, Y. Shimodaira, H. Kato, H. Kobayashi and A. Kudo, *Chem. Mater.*, 2008, **20**, 1299-1307.

9 M. Guan, C. Xiao, J. Zhang, S. Fan, R. An, Q. Cheng, J. Xie, M. Zhou, B. Ye and Y. Xie, *J. Am. Chem. Soc.*, 2013, **135**, 10411-10417.

10 J. X. Sun, G. Chen, Y. X. Li, R. C. Jin, Q. Wang and J. Pei, *Energy Environ. Sci.*, 2011, **4**, 4052-4060.



 